Physica A 187 (1992) 55–70
North-Holland

PHYSICA A

Microstructural sensitivity of local porosity distributions

F. Boger[a], J. Feder[a], T. Jøssang[a] and R. Hilfer[a,b]
[a]*Department of Physics, University of Oslo, 0316 Oslo, Norway*
[b]*Institut für Physik, Universität Mainz, W-6500 Mainz, Germany*

Received 4 December 1991
Revised manuscript received 13 February 1992

The recently introduced concept of local porosity distributions for the geometric characterization of arbitrary porous media is scrutinized using computer generated pore space images. The paper presents the first direct determination of local porosity distributions from digital images. Pore space images with identical two point correlation functions are employed to analyse the geometrical sensitivity of the local porosity concept. The main finding is that local distributions can be used to discriminate between images which are indistinguishable using standard correlation functions. We also discuss the question of length scales associated with the local porosity concept.

1. Introduction

A recent study [1, 2] has proposed a novel statistical characterization for the pore space geometry of arbitrary porous media. Apart from the intrinsic interest in better geometric descriptions of porous media the new characterization can be conveniently used for mean field calculations of physical properties. In ref. [1] such a mean field treatment was given for the frequency-dependent complex dielectric constant and in ref. [2] the permeability of porous media was investigated. Both studies produced new insights into, and remarkably good agreement with, well known experimental facts such as Archie's law, permeability–porosity relationships, conductivity–permeability correlations or dielectric enhancement. The key quantities in the new geometric characterization of porous media are local porosity distributions (or more generally local geometry distributions). Although the conceptual basis and measurement procedue for these quantities was described in detail in refs. [1, 2] no actual experimental observation was undertaken in those papers. Because the theoretical results of refs. [1, 2] for the dielectric and flow properties of porous media appear to be in agreement with experiment the direct determination and

further discussion of the underlying geometric characterization becomes of primary interest.

Measurements of local porosity distributions from digital images are reported for the first time in the present paper. In addition the present paper aims to evaluate and discuss the measurement procedure itself. Most importantly, however, the paper analyses the microstructural sensitivity and possible limitations of the local porosity concept.

Despite the fact that local porosity distributions were introduced in an attempt to study naturally occurring porous media such as sedimentary rocks the present paper will focus more on general image analysis than on the physics of porous media. The reason is our objective to study the microstructural sensitivity of the local porosity concept itself. Such a study must precede further use or discussion of the concept and has not yet been carried out. Because computer generated images can be produced easily in a controlled fashion they are much better suited for such an investigation than thin sections of naturally occurring porous media.

2. Definition of local porosity distributions

Geometrical characterization of porous media has in practice been limited to a few numbers [3, 4] such as porosity ϕ and specific internal surface area S. The porosity is defined as the ratio of pore space volume to total volume. The specific internal surface is the ratio between the surface area of the interface separating pore space and matrix space to the total volume. A better statistical characterization of porous media has focussed on the intuitive concept of pore size distribution [3, 4]. However, as discussed at length by Scheidegger [3] and Dullien [4], the concept is restricted to exceptional cases (such as the tube model) in which the pore sizes can be determined without ambiguity. Correlation functions for systems with an arbitrary stochastic geometry have not found wide application because the general n-point distribution functions [5] needed to calculate physical properties are extremely difficult to observe or measure from experiment. It is therefore of interest to find alternative statistical descriptions of porous media. Such an alternative was introduced in ref. [1] under the name of local porosity distribution and this concept will be defined next.

Let us consider a homogeneously and isotropically disordered pore space. We imagine the vertices of a Bravais lattice superposed on it. A primitive cell is associated with each lattice point $\boldsymbol{R}$. Let $G_{\mathrm{MC}}(\boldsymbol{R})$ denote the set of all points inside a cell at the lattice site $\boldsymbol{R}$. The index MC stands for "measurement cell". We denote by G_{PS} the set of all points in the pore space, and by ∂G_{PS} its

boundary. Then we define $\partial G_{PS} \cap G_{MC}(\boldsymbol{R})$ to be the "local geometry" associated with the lattice site $\boldsymbol{R}$. If ρ is the density of Bravais lattice points then $V_{MC} = 1/\rho$ is the volume of the measurement cell and this defines the length scale of resolution L as $L = \rho^{-1/3} = (V_{MC})^{1/3}$. For the simple cubic lattice with cubic primitive cell, L is the lattice constant. We have now defined the concept of local geometries for arbitrary topologically or continuously disordered pore spaces. For the case of substitutional disorder we identify the lattice of measurement cells with the underlying lattice.

The local geometry inside the measurement cell will become increasingly complex as the length scale of resolution L is increased. At every L the local geometry may be partially characterized by a few geometrical observables. The basic idea of local porosity distributions (or more generally local geometry distributions) is to turn a global geometric quantity into a distributed local observable. In this paper we focus exclusively on the case in which the porosity itself becomes a local concept.

To define the local or cell porosity we introduce the characteristic (indicator) function of an arbitrary set A as

$$\chi_A(\boldsymbol{r}) = \begin{cases} 0 & \text{if } \boldsymbol{r} \text{ lies outside the set A}, \\ 1 & \text{if } \boldsymbol{r} \text{ lies inside the set A}. \end{cases} \tag{2.1}$$

The local (or cell) porosity $\phi(\boldsymbol{R}, L)$ at the lattice position $\boldsymbol{R}$ and length scale L is then defined as

$$\phi(\boldsymbol{R}, L) = \rho \int \chi_{MC}(\boldsymbol{r}; \boldsymbol{R}, L)\, \chi_{PS}(\boldsymbol{r})\, \mathrm{d}^3\boldsymbol{r}, \tag{2.2}$$

where $\chi_{MC}(\boldsymbol{r}; \boldsymbol{R}, L)$ is the characteristic function of the measurement cell at $\boldsymbol{R}$ having size L, $\chi_{PS}(\boldsymbol{r})$ is the characteristic function of the pore space, and the integration extends over the porous medium. It is now straightforward to define local porosity distribution functions. In general the n-cell local porosity distribution function $\mu_n(\phi_1, \boldsymbol{R}_1; \ldots; \phi_n, \boldsymbol{R}_n; L)$ at scale L is the probability density to find local porosity ϕ_1 in the cell situated at $\boldsymbol{R}_1$, porosity ϕ_2 in the cell at $\boldsymbol{R}_2$ and so on. In the following we will be mostly interested in the case $n = 1$. Because we assumed the porous medium to be homogeneous we may write $\mu_1(\phi, \boldsymbol{R}; L) = \mu(\phi; L)$ for the 1-cell distribution function. The bulk porosity $\bar{\phi}$ is obtained by integrating over a large volume or by averaging over a statistical ensemble of measurement cells, and thus

$$\bar{\phi} = \phi(\boldsymbol{R}, L \to \infty) = \int_0^1 \phi \mu(\phi; L)\, \mathrm{d}\phi \tag{2.3}$$

independent of $\boldsymbol{R}$ and L.

The local porosity distribution $\mu(\phi; L)$ depends strongly on L. At small L the local geometries are simple. But they are highly correlated with each other. The one-cell function $\mu(\phi; L)$ at small L does not contain these complex geometric correlations. At large L the local geometries are statistically uncorrelated but each one of them is nearly as complex as the geometry of the full pore space. There must then exist an intermediate length scale L^* at which on the one hand the local geometries are relatively simple, and on the other hand the single cell distribution function has sufficient nontrivial geometric content to be a good first approximation. For systems with an underlying lattice symmetry the length L^* is simply chosen to be the lattice constant of the uderlying lattice. For other systems several methods to determine L^* present themselves:

(1) The entropy method. The entropy method attempts to formalize the intuitive considerations above. The idea is to maximize the geometrical content contained in $\mu(\phi; L)$ or equivalently to minimize the information function

$$S(L) = \int_0^1 \mu(\phi; L) \log \mu(\phi; L)\, \mathrm{d}\phi \,. \tag{2.4}$$

The length scale $L^* = \xi_S$ is then determined through the condition $\mathrm{d}S/\mathrm{d}L|_{L=\xi_S} = 0$.

(2) The correlation method. This method is based on the porosity autocorrelation function at scale L given as

$$C(R, L) = \frac{\int_0^1 \int_0^1 (\phi_1 - \bar{\phi})(\phi_2 - \bar{\phi})\mu_2(\phi_1, \phi_2; R; L)\, \mathrm{d}\phi_1\, \mathrm{d}\phi_2}{\int_0^1 (\phi - \bar{\phi})^2 \mu(\phi; L)\, \mathrm{d}\phi} \,, \tag{2.5}$$

where the function $\mu_2(\phi_1, \phi_2; R; L) = \mu_2(\phi_1, \boldsymbol{R}_1; \boldsymbol{R}_2; L)$ depends only on the distance $R = |\boldsymbol{R}_1 - \boldsymbol{R}_2|$ by homogeneity. There are several possibilities to extract a correlation length from $C(R) = C(R, L = 0)$. A generally applicable procedure is to use the value of R at which $C(R)$ has dropped to $1/\mathrm{e}$. Thus the length $L^* = \xi_C$ is defined through the condition $C(\xi_C) = 1/\mathrm{e}$. Note that there are other methods to determine a correlation length from $C(R)$. Our particular choice has the virtues of simplicity and generality.

(3) The experimental method. Here the idea is to keep L a free parameter in all calculations, and to adjust it by comparison with experiment. This method of determining L^* will not be considered here.

We conclude this section with a brief discussion of the difference between our measurement cell and the so-called representative elementary volume [6], which has been introduced in order to pass from a set of microscopic equations to macroscopic ones. The condition for a length scale L_{REV} to qualify as the typical length scale for a representative elementary volume can in the present language be formulated as $\partial\phi(\boldsymbol{R}, L)/\partial L = 0$ at L_{REV}. This condition is not satisfied for L^*, in fact one has $L_{\mathrm{REV}} \gg L^*$. The length scale of a representative elementary volume is macroscopic while our measurement cells are *mesoscopic*.

3. Measurability of local porosity distributions

The most important aspect of $\mu(\phi) = \mu(\phi; L^*)$ is that it is readily measurable using modern image processing equipment. In the following a simplified and approximate procedure to observe $\mu(\phi)$ in continuously disordered homogeneous and isotropic porous media will be discussed. This procedure measures $\mu(\phi)$ from photographs of two-dimensional thin sections through the pore space. These photographs must be coloured such that pore space and matrix are clearly distinguished. The quality of the pore space visualization should be such that a high resolution digitization of the image allows each pixel to be assigned unambiguously to either pore space or matrix.

The next step is to choose a length scale of resolution L, and to subdivide the photograph into cells by placing, e.g., a square grid with squares of length L over it. The local porosities inside the cells may now be calculated by noting that $\lim_{L\to 0} \phi(\boldsymbol{R}, L)$ corresponds to the pixel value 0 or 1 according to whether the pixel at position $\boldsymbol{R}$ falls into matrix (0) or pore space (1). The cell porosities are then

$$\phi_i = \frac{1}{L^2} \sum_{j=1}^{L^2} \phi_i(\boldsymbol{R}_j) , \tag{3.1}$$

where $\phi_i(\boldsymbol{R}_j)$ is the pixel at position $\boldsymbol{R}_j$ within cell i. The resulting probability density is averaged over different ways of placing the measurement lattice, over many choices of the primitive cell, and over all available photographs of two-dimensional sections to obtain the local porosity density $\mu(\phi)$.

At this point it is pertinent to ask whether $\mu(\phi; L)$ may be calculated simply from two-dimensional sections through the porous medium. In the following we present an argument that this is indeed the case. Consider a cut plane $P(\boldsymbol{n}, y)$ through the pore space determined through its unit normal $\boldsymbol{n}$ and an offset y. The area of pore space on a particular cut plane is given by

$$A(\boldsymbol{n}, y) = \int_{P(\boldsymbol{n}, y)} \chi_{PS}(\boldsymbol{r})\, \mathrm{d}^2\boldsymbol{r}\,, \tag{3.2}$$

where the integration extends over the whole plane. The porosity determined from such a cut is then $\phi'(\boldsymbol{n}, y) = A(\boldsymbol{n}, y)/L_S^2$ where L_S is the system size. The average porosity obtained from averaging over y is then

$$\langle \phi'(\boldsymbol{n}) \rangle = \frac{1}{L_S} \int A(\boldsymbol{n}, y)\, \mathrm{d}y\,. \tag{3.3}$$

Now using that

$$\frac{1}{4\pi} \int\int \int_{P(\boldsymbol{n}, y)} \chi_{PS}(\boldsymbol{r})\, \mathrm{d}^2\boldsymbol{r}\, \mathrm{d}y\, \mathrm{d}\boldsymbol{n} = \int \chi_{PS}(\boldsymbol{r})\, \mathrm{d}^3\boldsymbol{r}$$

because of isotropy, one arrives at

$$\langle \phi'(\boldsymbol{n}) \rangle = \frac{1}{L_S^3} \int \chi_{PS}(\boldsymbol{r})\, \mathrm{d}^3\boldsymbol{r} = \bar{\phi} \tag{3.4}$$

independent of $\boldsymbol{n}$. Further averaging over the possible directions $\boldsymbol{n}$ does not change this result.

The porosity autocorrelation function $C(R)$ can be calculated from the pixel power spectrum using the Wiener–Khintchine theorem. Inverse Fourier transform of the power spectrum gives the two-dimensional pixel autocorrelation function. Averaging with respect to the angular variable at fixed radius R yields then $C(R)$.

The result of the measuring procedure described in the preceding paragraphs will in general lead to a local porosity distribution of the form

$$\mu(\phi, L) = \mu_0(L)\, \delta(\phi) + [1 - \mu_0(L) - \mu_1(L)]\tilde{\mu}(\phi, L) + \mu_1(L)\, \delta(\phi - 1)\,. \tag{3.5}$$

Its bulk (average) porosity $\bar{\phi}$ is obtained as the expectation value $\bar{\phi} = \int_0^1 \phi\mu(\phi, L)\, \mathrm{d}\phi$ in agreement with eq. (2.3). The one parameter family of local porosity distribution $\mu(\phi, L)$ contains very much geometrical information about the pore space geometry. The choice of a particular mesoscopic scale L^* implies that $\mu(\phi, L^*)$ contains an optimal amount of information based purely on the porosity concept. If the cells were chosen much larger than L^*, then the simple form

$$\mu(\phi; L \gg L^*) = \delta(\phi - \bar{\phi}) \tag{3.6}$$

is expected to result. In this limit the geometric information is reduced to $\bar{\phi}$. At the same time the local geometries are nearly as complex as the bulk geometry. If on the other hand the cells are chosen very small, i.e. $L \ll L^*$, then the measurement procedure above could still be applied and is expected to yield

$$\mu(\phi; l \ll L^*) = \bar{\phi}\delta(\phi - 1) + (1 - \bar{\phi})\delta(\phi) . \tag{3.7}$$

Again the geometrical information is reduced to one number. The geometrical complexity has disappeared into the correlations between cells which are not contained in the single cell quantity $\mu(\phi, L)$.

The local porosity distribution $\mu(\phi) = \mu(\phi, L^*)$ is easily calculated for ordered or substitutionally disordered porous media, but very difficult to obtain for the topological or continuum disorder. For ordered or substitutionally disordered cases the measurement lattice is given by the underlying lattice, and L^* is the lattice constant. One finds immediately $\mu(\phi) = \delta(\phi - \bar{\phi})$ for the ordered case. For substitutional disorder the local porosity density follows directly from the distribution of the individual geometrical elements which occupy the lattice sites.

4. Description of test images

In this section we describe the creation of the artificial thin sections displayed in fig. 1. The selection of these images was guided by our objective to explore the range of applicability and to test the limitations of the local porosity concept.

Two methods were used in the creation of the four images of fig. 1, which may be distinguished as real space (fig. 1a–c) respectively Fourier space methods (fig. 1d).

In the real space method we start by filling a 512×512 array with random numbers drawn from a normal distribution with unit variance. Next we specify a filter with size ξ_F and given shape. We have employed three different filters whose shape fits inside a square of side length $\xi_F = 15$. The first filter simply had the shape of the full square. The second was obtained by inscription of a circle with radius ξ_F into the square. The third filter shape was obtained by inscribing an L whose two arms had the length $\xi_F = 15$ and thickness 7. Next the array of random numbers is smoothed by centering the filter on top of a given array element and averaging over all random numbers selected by the filter shape. The resulting average then replaces the original random number at the chosen array element. This procedure is repeated for all array elements using periodic boundary conditions whenever necessary. The result is a

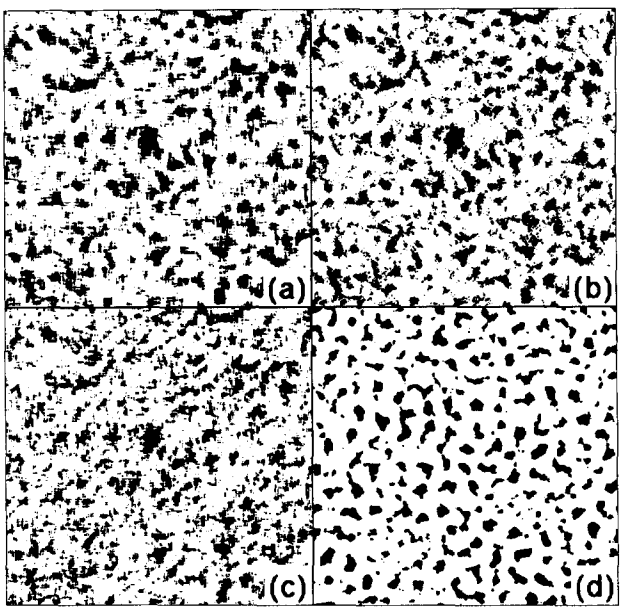

Fig. 1. Computer generated images of pore space configurations. The pore space is indicated black. The bulk porosity in all four images is $\bar{\phi} \approx 0.195$. (a) was created by real space filtering using a square filter. (b) was created by real space filtering using a circular filter. (c) was created by real space filtering using an L-shaped filter. (d) was created by Fourier space filtering. The filter size in all four cases is $\xi_F = 15$. The resolution in all images is 512×512 pixels.

smoothed 512×512 array of random numbers. This array is transformed into an array of 0's and 1's by chosing a threshold value such that a predefined fraction of pixels has the value 1. In our case we chose this fraction to be 0.2. The pixel value 1 is represented black, the pixel value 0 is represented white. The results are shown in fig. 1a–c. Note that we used the *same* realization of random numbers in all three images.

The Fourier space method starts also from an array of random real numbers, which are now interpreted as random Fourier components. They are smoothed by multiplication with a function $f(\boldsymbol{k})$ such that $f(\boldsymbol{k}) = 0$ for $|\boldsymbol{k}| < k_0$ and $f(\boldsymbol{k}) = |\boldsymbol{k}|^{-\beta}$ for $|\boldsymbol{k}| \geq k_0$. The resulting array is Fourier transformed and then discriminated into 0's and 1's using a suitable threshold value as before. The image of fig. 1d corresponds to parameters $k_0 = 12$ and $\beta = 5$.

5. Results and discussion

Fig. 2 displays the two point correlation function $C(R)$ for the images of fig. 1. The curve with solid circles connected by a dashed line has a clear minimum

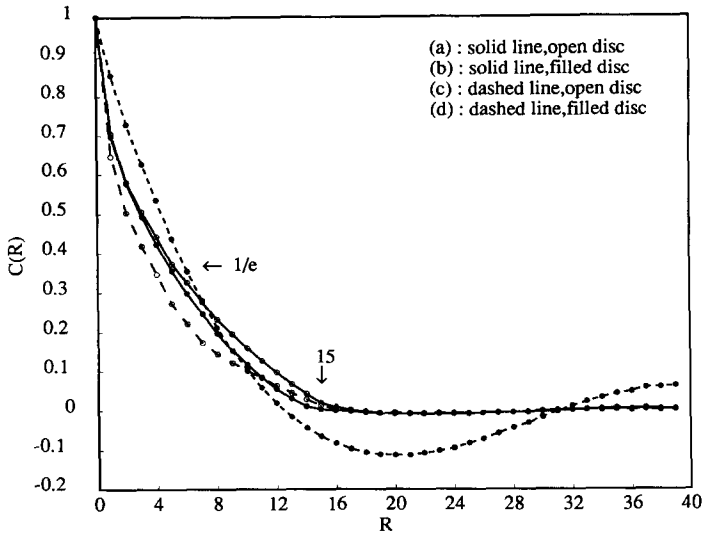

Fig. 2. Pixel–pixel-correlation functions for the images in fig. 1. The solid line with open symbols corresponds to image (1a), the solid line with solid symbols to image (1b), the dashed line with open symbols to image (1c) and the dashed line with solid symbols to image (1d).

and corresponds to the image (d). The real space filtered images (a) through (c) are nearly indistinguishable beyond the filter size $\xi_F = 15$. This reflects their visual similarity and is a result of using the same random field underlying the filtering process. We obtain the correlation lengths $\xi_C^a = 6$, $\xi_C^b = 5$, $\xi_C^c = 4$ and $\xi_C^d = 6$ for the four cases. The correlation functions (a) through (c) show only a flat minimum because of the roughness of the pore space boundary. The most important conclusion to be drawn from fig. 2 is that any theoretical approach which uses correlation functions to characterize the configurations cannot distinguish between the images (a) through (c).

The one parameter family of local porosity densities $\mu(\phi, L)$ was calculated along the lines of sections 2 and 3. We have used a quadratic and a rectangular lattice of measurement cells. Because the results were similar we present them only for the quadratic case. We averaged over all possible positions of the lattice using periodic boundary conditions, but we did not average over different orientations. The resulting probability densities for measurement cells with side lengths $L = 5, 10, 15, \ldots, 45$ are displayed in fig. 3. The data have been binned into bins of size 0.01. The data points are assigned to the left end of the interval. In fig. 4 we plot the information function $S(L)$ calculated from eq. (2.4). From $S(L)$ we find the entropy lengths to be $\xi_S^a = 22$, $\xi_S^b = 19$, $\xi_S^c = 20$ and $\xi_S^d = 21$. Finally, in fig. 5 we collect the local porosity densities with L^* determined from the entropy method into a single plot.

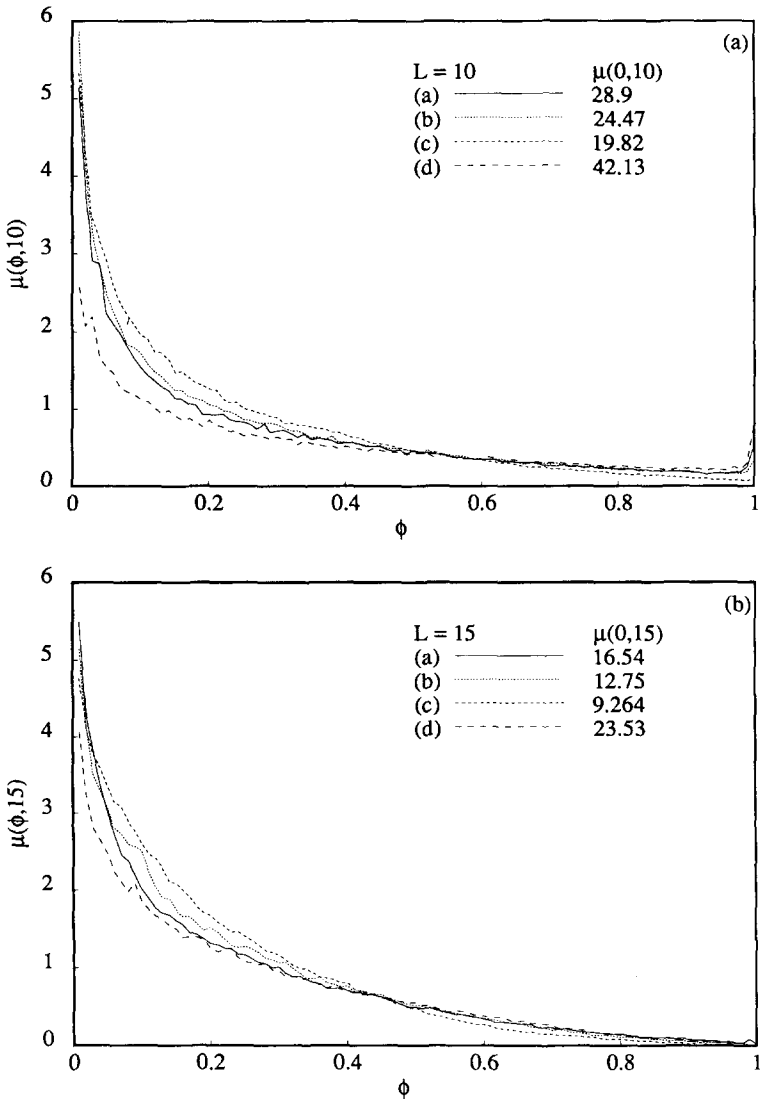

Fig. 3. Local porosity density functions $\mu(\phi, L)$ for the images of fig. 1. Solid line corresponds to image (1a), short dashed to image (1b), medium dashed to image (1c), long dashed to image (1d). The results displayed are for measurement cells of side length $L = 10$ in (a), $L = 15$ in (b), $L = 20$ in (c), $L = 25$ in (d), $L = 30$ in (e), $L = 35$ in (f), $L = 40$ in (g) and $L = 45$ in (h).

The first observation from fig. 3 is that the local porosity densities show indeed the expected crossover from being concentrated at the origin and at 1 for small L to being concentrated around $\bar{\phi}$ for large L. The crossover length is found to range close to the entropy length determined from fig. 4. There appears to be considerable statistical uncertainty reflected in the roughness of

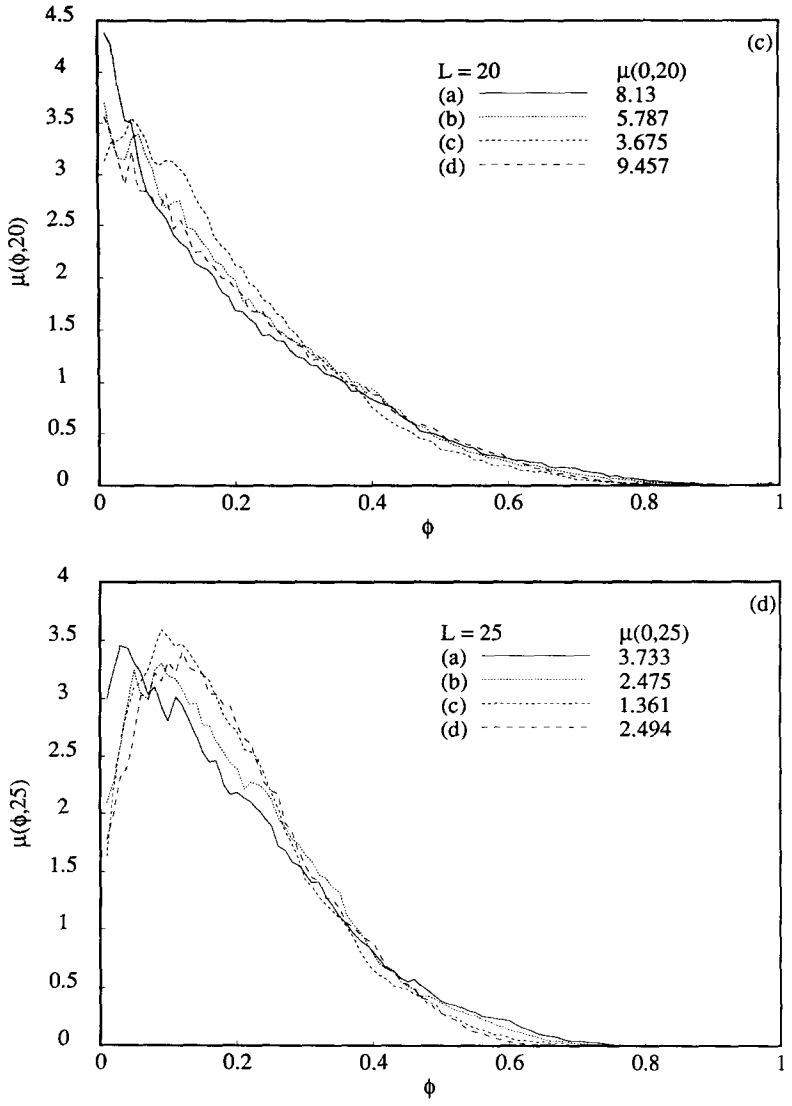

Fig. 3 (cont.).

the curves which results from the relatively coarse digitization of 512×512 pixels.

The most important observation from figs. 3, 4 and 5 is that the local porosity approach is more sensitive in distinguishing between different images than the correlation function approach. The local porosity densities displayed in fig. 3 show characteristic differences between the images which are directly

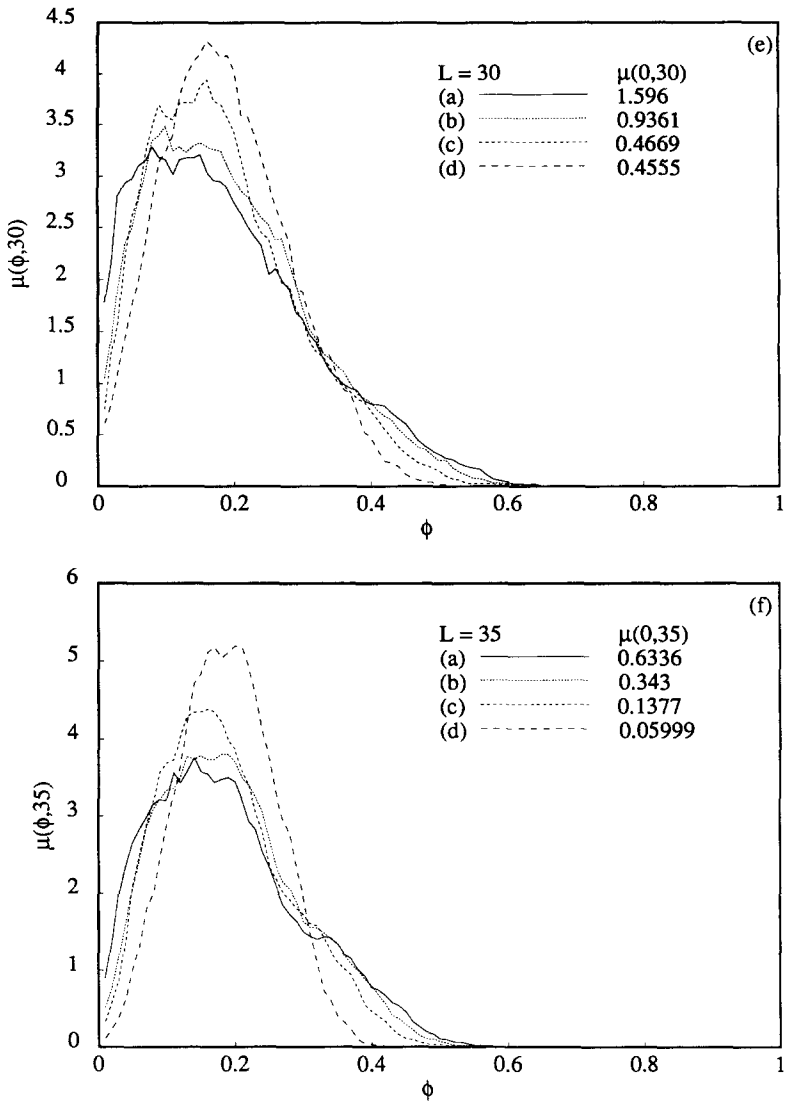

Fig. 3 (cont.).

related to visual features. The sensitivity of the local porosity distribution is most clearly seen by comparing the medium dashed curve for image (c) with those for image (a) (solid curve) and image (b) (narrow dashed curve). The curves for image (c) are clearly different beyond the statistical uncertainty even at values of L which are much larger than ξ_F such as $L = 30$. The reader should keep in mind that image (c) differs from (a) and (b) only in the filter shape.

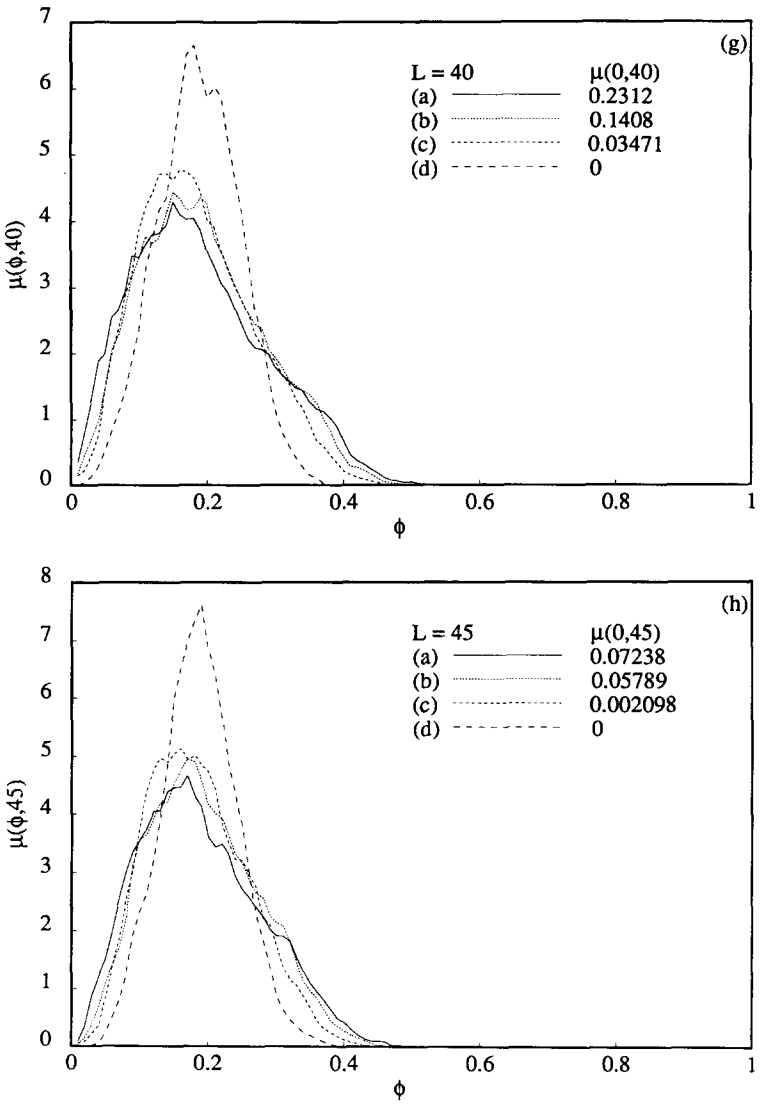

Fig. 3 (cont.).

The differences between images (a) and (b) are less pronounced and higher resolution images giving better statistics might show that the filter shapes are not sufficiently different. From our data however, there appears to be a significant distinction in the low porosity regime for intermediate values of L. We think that the slightly smoother pore space boundary of image (a) reflects itself in a somewhat larger fraction of small porosity regimes for $L = 20$ and

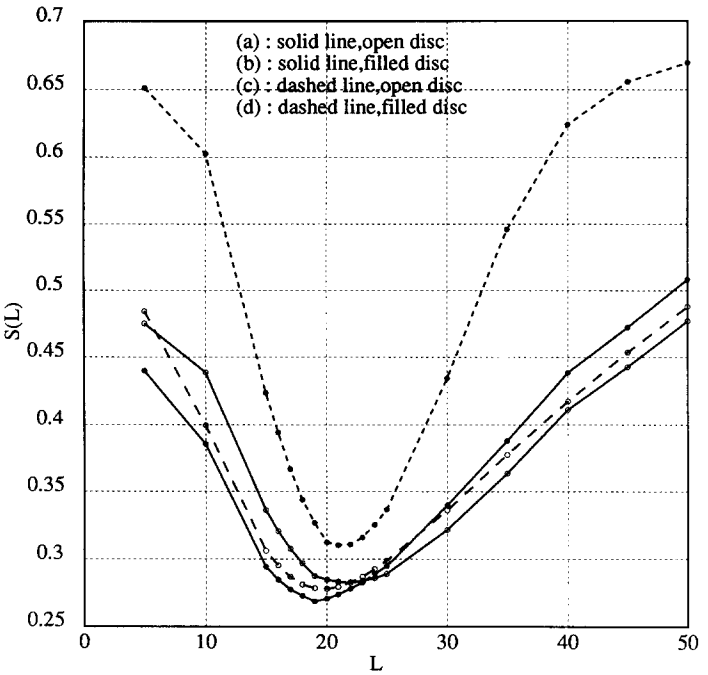

Fig. 4. Entropy function $S(L)$ as a function of the length of the measurement cell. The line styles are those of fig. 2.

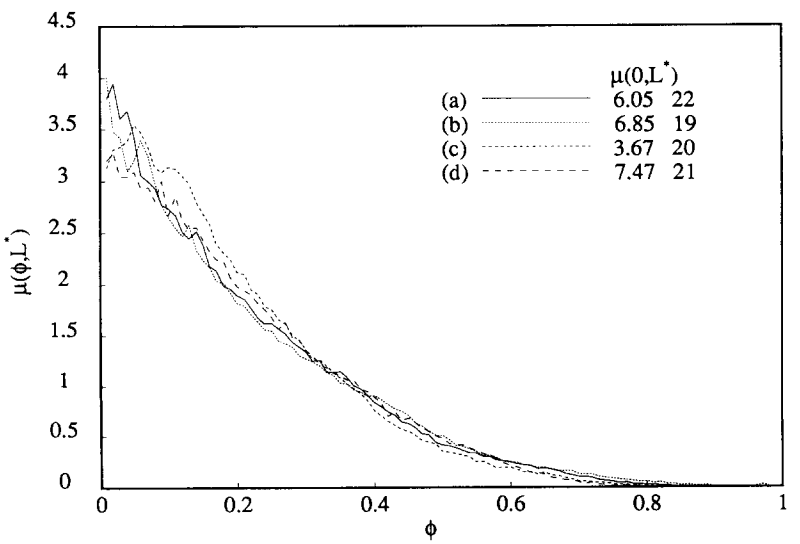

Fig. 5. Local porosity density functions $\mu(\phi, L)$ with $L = L^* = \xi_S$ for the images of fig. 1. Solid line corresponds to image (1a) with $\xi_S^a = 22$, short dashed to image (1b) with $\xi_S^b = 19$, medium dashed to image (1c) with $\xi_S^c = 20$, long dashed to image (1d) with $\xi_S^d = 21$.

$L = 25$. Note also that curves (a) and (b) appear to exhibit signs of bimodality although this effect is probably statistically insignificant.

The information function displayed in fig. 4 also reveal considerable geometric sensitivity. In particular the two most similar pictures (a) and (b) exhibit the largest difference in their entropy lengths, $\xi_S^a > \xi_S^b$. This appears to resemble the fact that the square filter extends beyond the circular one in the diagonal direction. Note also that the entropy lengths determined from fig. 4 are consistently larger than the correlation lengths ξ_C determined from fig. 2.

Fig. 5 shows the local porosity distributions $\mu(\phi, L^*)$ for the suggested choices of $L^* = \xi_S$. While curve (c) is still significantly different from (a) and (b) the difference between the latter two curves appears to vanish. Here we encounter naturally the limitations for the sensitivity of the local porosity distributions. Two images created from an identical field of random numbers by very similar filters can no longer be distinguished. We emphasize that in our opinion more measurements of local porosity distributions are needed before the degree of statistical uncertainty of such data is clarified. Because of this it is also premature to settle on an "optimal" choice for L^*. Unless a particular choice is made the full one parameter family $\mu(\phi, L)$ of distributions should be considered.

6. Conclusion

The local porosity approach to characterize the stochastic geometry of porous media was scrutinized in this paper. We have presented the first measurements of local porosity distributions from digital images. At the same time we have put the geometric sensitivity of local porosity distributions to a rather severe test. We find that the local porosity concept appears to be surprisingly sensitive to geometric features. However, more studies along the same lines are necessary to further explore the limits of this sensitivity. Such studies are also desirable in view of the fact that local porosities provide a theoretical framework inside which the nature of empirical scaling relations for the physical properties of porous media can be understood on the basis of the microgeometry [1, 2]. Measurement of local porosity distributions and local percolation probabilities from laboratory samples will allow quantitative comparison of the theory with experiment.

Acknowledgement

We thank the German–Norwegian Research and Development Programme (Project B-2) for financial support.

References

[1] R. Hilfer, Phys. Rev. B 44 (1991) 60.
[2] R. Hilfer, Phys. Rev. B, in press.
[3] A.E. Scheidegger, The Physics of Flow Through Porous Media (Univ. of Toronto Press, Toronto, 1974).
[4] F.A.L. Dullien, Porous Media: Fluid Transport and Pore Structure (Academic Press, New York, 1979).
[5] S. Torquato, J. Stat. Phys. 45 (1986) 843.
[6] J. Bear and Y. Bachmat, Introduction to Modeling of Transport Phenomena in Porous Media (Kluwer, Dordrecht, 1990).